

Electronic Supplementary Information

**Solvent-dependent access to mono- and dinuclear copper(II)
assemblies based on a flexible imidazole ligand**

A. A. Kitos,^a E. E. Moushi,^b M. J. Manos,^b C. Papatriantafyllopoulou,^b A. J. Tasiopoulos,^{*b}
S. P. Perlepes^a and V. Nastopoulos^{*a}

^a Department of Chemistry, University of Patras, 26504 Patras, Greece

^b Department of Chemistry, University of Cyprus, 1678 Nicosia, Cyprus

Table S1. Geometry (\AA , $^{\circ}$) of the strong hydrogen-bonding motifs in compounds **1a**·2MeOH–**5**^a

D–H···A	D–H	H···A	D···A	\angle (DHA)
1a ·2MeOH				
N1A–H1A···O4 ⁱ	0.86(2)	1.99(2)	2.851(2)	177(2)
N1B–H1B···O5 ⁱⁱ	0.86(2)	1.95(2)	2.795(2)	168(2)
O5–H5···O3	0.85(2)	1.95(2)	2.788(2)	170(2)
1b				
N1A–H1A···O3 ⁱⁱⁱ	0.86(4)	1.94(4)	2.729(4)	152(3)
N1B–H1B···O6 ^{iv}	0.85(3)	1.94(3)	2.782(5)	174(5)
N1C–H1C···O2 ^v	0.84(4)	1.94(4)	2.778(4)	176(5)
N1D–H1D···O4 ^{vi}	0.85(3)	1.97(4)	2.783(5)	160(3)
2a				
N1A–H1A···O2	0.87(2)	2.09(2)	2.925(3)	161(2)
N1B–H1B···O3 ⁱ	0.86(2)	2.02(2)	2.867(3)	170(3)
2b				
N1A–H1A···O4 ^{vii}	0.85(3)	2.03(3)	2.873(4)	172(4)
N1B–H1B···O4 ^{viii}	0.86(3)	2.08(3)	2.843(4)	149(3)
3				
N1A–H1A···F3A ^{ix}	0.85(3)	2.13(3)	2.927(9)	155(3)
N1A–H1A···F5 ^{ix}	0.85(3)	2.18(3)	2.891(3)	141(3)
N1B–H1B···F1A ^x	0.86(3)	1.90(3)	2.709(2)	157(3)
N1C–H1C···F3A	0.86(3)	2.10(3)	2.826(8)	142(3)
N1D–H1D···F1A ^{xi}	0.85(3)	2.16(3)	2.881(9)	143(3)
4				
N1A–H1A···O1 ^{xii}	0.87(2)	2.10(2)	2.949(3)	167(3)
N1B–H1B···O4 ^{xi}	0.86(2)	1.88(2)	2.735(3)	174(3)
5				
N1A–H1A···Cl ^{xiii}	0.85(2)	2.32(2)	3.154(2)	169(2)

^a Symmetry codes: (i) $1/2+x$, $1/2-y$, $1/2+z$; (ii) $1/2-x$, $1/2-y$, $1/2+z$; (iii) $-1/2+x$, $-1/2+y$, z ; (iv) $-1/2+x$, $1/2+y$, z ; (v) x , $1-y$, $-1/2+z$; (vi) x , $-y$, $-1/2+z$; (vii) x , $-1+y$, $-1+z$; (viii) $1/2-x$, $-1+y$, $-1/2+z$; (ix) $3/2-x$, $-1/2+y$, $3/2-z$; (x) $1/2-x$, $-1/2+y$, $3/2-z$; (xi) $1+x$, y , z ; (xii) $1-x$, $1/2+y$, $1/2-z$; (xiii) $-1/2+x$, $1/2-y$, $-z$.

Table S2. Weak hydrogen-bonding geometry (\AA , $^\circ$) in compounds **1a**·2MeOH–**5**^a

D–H···A	D–H	H···A	D···A	$\angle(\text{DHA})$	Symmetry operation of A		
1a ·2MeOH							
C11A–H11A···O4	0.93	2.61	3.313(2)	133	$1/2+x, 1/2-y, 1/2+z$		
C13–H13C···O3	0.96	2.65	3.510(3)	149	$2-x, 1-y, -z$		
1b							
C11A–H11A···O2	0.93	2.49	3.413(5)	173	$-1/2+x, -1/2+y, z$		
C8D–H8D···O5	0.93	2.50	3.341(6)	150	$-1/2+x, 1/2-y, -1/2+z$		
C11D–H11D···O6	0.93	2.42	3.340(5)	169	$x, -y, -1/2+z$		
C4B–H4B···O1	0.93	2.64	3.411(5)	141	x, y, z		
2a							
C4A–H4A···O4	0.93	2.44	3.367(3)	178	$2-x, -y, 1-z$		
C4B–H4B···O3	0.93	2.48	3.348(3)	156	$x, y, 1+z$		
2b							
C4B–H4B···O1	0.93	2.51	3.270(5)	139	$x, -1/2+y, -1/2+z$		
C8A–H8A···O2	0.93	2.56	3.183(4)	125	$1/2-x, -1/2+y, -1+z$		
C11A–H11A···O2	0.93	2.54	3.442(4)	164	$x, -1+y, -1+z$		
3							
C5B–H5B···F4A	0.93	2.55	3.170(15)	125	$1/2-x, -1/2+y, 3/2-z$		
C8A–H8A···F5	0.93	2.39	3.298(3)	165	$1/2+x, 1/2-y, -1/2+z$		
C8B–H8B···F2A	0.93	2.52	3.410(10)	162	$1/2+x, 1/2-y, 1/2+z$		
C8C–H8C···F6	0.93	2.45	3.374(4)	176	$1/2+x, 1/2-y, -1/2+z$		
C8D–H8D···F2A	0.93	2.41	3.260(9)	151	$1/2+x, 1/2-y, 1/2+z$		
C11A–H11A···F3A	0.93	2.46	3.288(9)	148	$3/2-x, -1/2+y, 3/2-z$		
4							
C11A–H11A···O4	0.93	2.56	3.438(3)	157	$1-x, 1/2+y, 1/2-z$		
C9B–H9B···O3	0.93	2.65	3.564(3)	169	$x, 1/2-y, 1/2+z$		
5							
C5A–H5A···Cl	0.93	2.94	3.707(3)	141	$3/2-x, -1/2+y, z$		
C9A–H9A···Cl	0.93	2.80	3.662(2)	154	$x, 1/2-y, -1/2+z$		
C–H···C _g	C–H	H···C _g	C···C _g	$\angle(\text{CHC}_g)$	H···(ring plane) distance	Offset [#]	Symmetry operation of C _g
1a ·2MeOH							
C5A–H5A···C _g ⁱ	0.93	2.71	3.488(3)	142	2.61	0.73	$5/2-x, -1/2+y, 1/2-z$
C5B–H5B···C _g ⁱⁱ	0.93	2.67	3.544(3)	156	2.61	0.56	$3/2-x, 1/2+y, 1/2-z$
2b							
C5A–H5A···C _g ⁱⁱ	0.93	2.65	3.539(5)	160	2.64	0.21	$-x, -1/2-y, -1/2+z$
C5B–H5B···C _g ⁱ	0.93	2.72	3.607(5)	159	2.66	0.57	$1/2-x, y, 1/2+z$
4							
C8B–H8B···C _g ⁱⁱⁱ	0.93	2.71	3.509(3)	144	2.70	0.18	$1-x, -1/2+y, 1/2-z$
5							
C11–H11···C _g ^{iv}	0.93	2.69	3.479(3)	143	2.69	0.10	$3/2-x, -1/2+y, z$

^a Ring centroids: (i) C6A to C11A; (ii) C6B to C11B; (iii) N1A to C5A; (iv) C6 to C11.

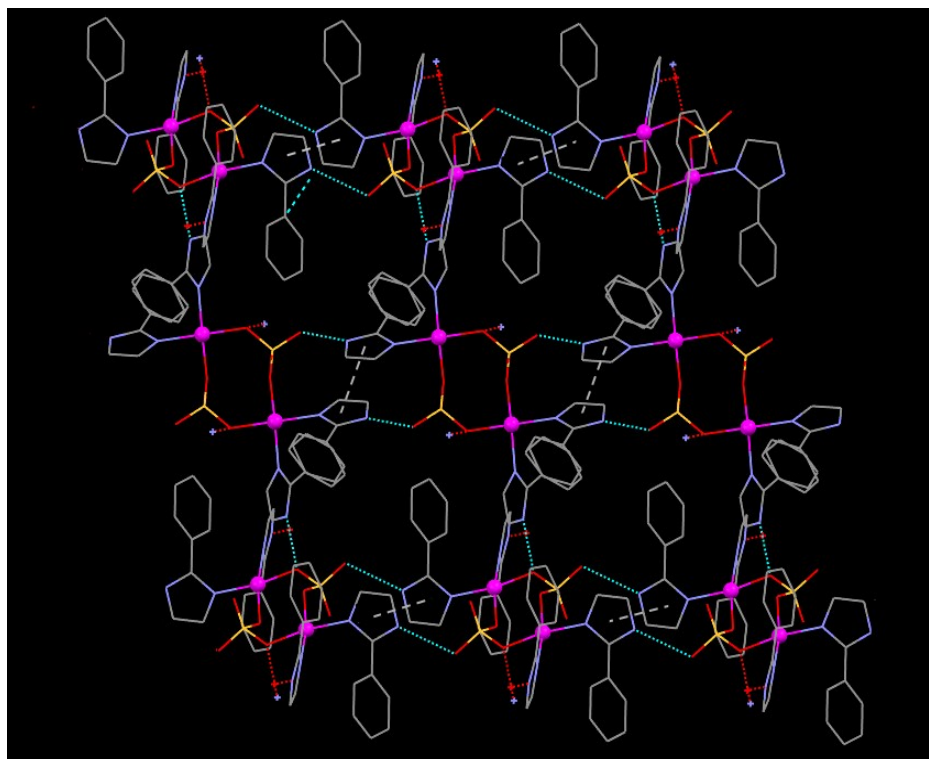
[#] The offset is the distance between the centroid C_g and the footprint of the projection of the H-atom on the ring plane.

Table S3. π - π stacking distances (\AA) and angles ($^\circ$) in compounds **1b–5^a**

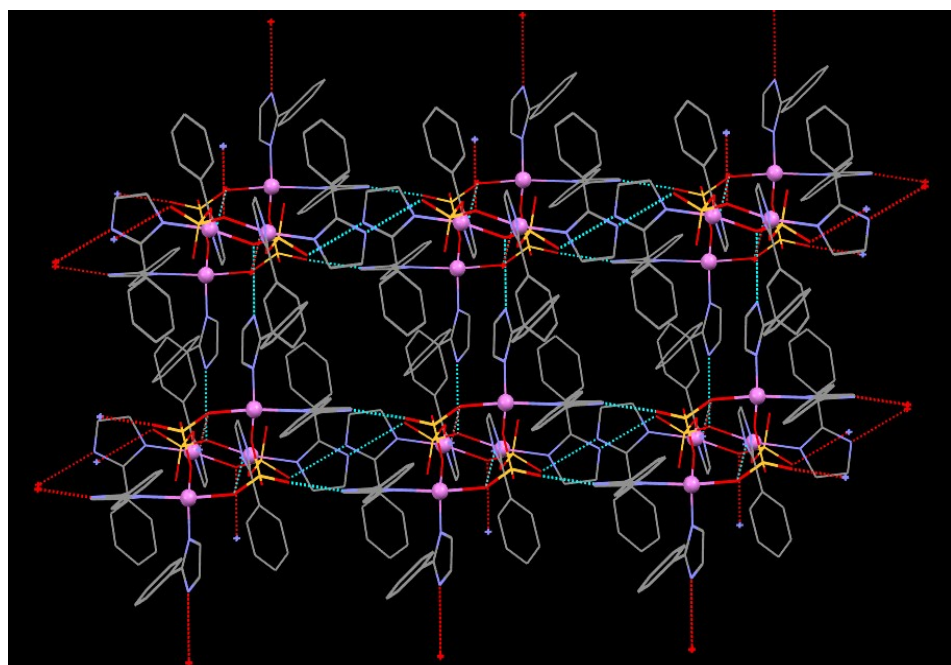
	Rings*	1b	2a	2b	3	4	5
Distance between ring centroids	A1–B2	3.502(3)	3.704(2)	3.547(2)			
	A2–B1	3.819(3)	3.616(2)	3.454(2)			
	C1–D2	3.806(3)					
	C2–D1	3.427(3)					
	B2–B2 ⁱ				3.550(3)		
	B1–B1 ⁱⁱ					3.648(3)	
	A1–A1 ⁱⁱⁱ						3.606(2)
Perpendicular distance between ring planes	A1–B2	3.443(3)	3.584(2)	3.517(2)			
	A2–B1	3.814(3)	3.451(2)	3.415(2)			
	C1–D2	3.805(3)					
	C2–D1	3.385(3)					
	B2–B2 ⁱ				3.482(3)		
	B1–B1 ⁱⁱ					3.327(3)	
	A1–A1 ⁱⁱⁱ						3.308(2)
Centroid offset	A1–B2	0.642(9)	0.934(5)	0.458(6)			
	A2–B1	0.208(9)	1.080(5)	0.519(7)			
	C1–D2	0.068(9)					
	C2–D1	0.532(8)					
	B2–B2 ⁱ				0.693(6)		
	B1–B1 ⁱⁱ					1.495(6)	
	A1–A1 ⁱⁱⁱ						1.434(6)
Dihedral angle between ring mean-planes	A1–B2	13.2(2)	17.4(1)	14.7(2)			
	A2–B1	27.4(2)	13.5(1)	11.3(2)			
	C1–D2	25.1(2)					
	C2–D1	12.5(2)					
	B2–B2 ⁱ				0.0		
	B1–B1 ⁱⁱ					0.0	
	A1–A1 ⁱⁱⁱ						3.7(2)

^a Symmetry codes: (i) 1– x , − y , 2– z ; (ii) 2– x , − y , 1– z ; (iii) 3/2– x , −1/2+ y , z .

* Rings A1/B1/C1/D1 and A2/B2/C2/D2 refer to the imidazole and the phenyl rings of the ligands of the complexes, respectively.



(a)



(b)

Figure S1. Supramolecular features in the crystal structure of complex [Cu₂(SO₄)₂(LH)₄] (**4**). (a) Strong N–H \cdots O(SO₄²⁻) interactions (cyan dotted lines) give rise to robust layers, further stabilised by aromatic π \cdots π stackings (grey dashed lines). Adjacent layers are interlinked by additional N–H \cdots O(SO₄²⁻) interactions (red hanging contacts) towards a 3D assembly. (b) Extended packing of **4** showing the stacking arrangement of two such adjacent supramolecular layers. Hydrogen atoms have been omitted.

IR Discussion

IR data are shown in Fig. S2. The IR spectra of the complexes exhibit a medium to strong broad band above 3130 cm⁻¹ attributable to the $\nu(\text{NH})$ vibration of the coordinated LH ligand; this vibration appears at 3418 cm⁻¹ in the spectrum of the free ligand.

The spectra of **2a** and **2b** exhibit two strong bands at ~1100 and 622 cm⁻¹, due to the $\nu_3(F_2)[\nu_{\text{d}}(\text{Cl-O})]$ and $\nu_4(F_2)[\delta_{\text{d}}(\text{OCLO})]$ modes, respectively, of the uncoordinated T_{d} ClO₄⁻ counterions;¹ the former has also a deformation aromatic ring character as proven by its appearance in the spectra of the other complexes (at 1104 cm⁻¹ in free LH). The spectrum of **3** shows a strong band at 776 cm⁻¹ and a medium-intensity one at 476 cm⁻¹ attributable to the $\nu_3(F_{1\text{u}})[\nu(\text{Si-F})]$ and $\nu_4(F_{1\text{u}})[\delta(\text{FSiF})]$ IR-active vibrations, respectively, of the uncoordinated octahedral (O_{h}) SiF₆²⁻ counterion,¹ the former band again having a coordinated LH bending character. The IR spectrum of the free, i.e. ionic, sulfate (the ion belongs to the T_{d} point group) consists of two bands at ~1100 and ~615 cm⁻¹, assigned to the $\nu_3(F_2)[\nu_{\text{d}}(\text{S-O})]$ and $\nu_4(F_2)[\delta_{\text{d}}(\text{OSO})]$ modes, respectively.^{1,2} Coordination of SO₄²⁻ to metal ions decreases the symmetry of the group, and the ν_3 and ν_4 modes are split.^{1,2} Furthermore, the Raman-active stretching $\nu_1(A_1)[\nu_{\text{d}}(\text{S-O})]$ and bending $\nu_2(E)[\delta_{\text{d}}(\text{OSO})]$ modes of the free SO₄²⁻ become IR-active upon coordination, i.e. once the symmetry is lowered. In the case the SO₄²⁻-site symmetry is lowered from T_{d} to $C_{2\text{v}}$ (bidentate chelating or bridging coordination), both ν_1 and ν_2 appear in the IR spectrum, while ν_3 and ν_4 each splits into three IR-active vibrations.¹ Complex **4** has $C_{2\text{v}}$ symmetry at the sulfato ligand, and the IR bands at 1054, 1076 and 1216 cm⁻¹ are therefore attributable to the ν_3 modes.¹ The bands at 584, 605 and 716 cm⁻¹ are assigned to the ν_4 modes.¹ The bands at 970 and 444 cm⁻¹ are assigned to the ν_1 and ν_2 modes, respectively, with the higher wavenumber band being superimposed by a ligand vibration. The spectrum of **1b** exhibits a very strong band at 1384 cm⁻¹ assigned¹ to the $\nu_3(E')[\nu_{\text{d}}(\text{N-O})]$ mode of the $D_{3\text{h}}$ ionic nitrates that are present as counterions in the crystal structure of the complex. Rather surprisingly the KBr IR spectra of **1a** and **1b** are almost identical in the 1250-1550 cm⁻¹ region. The spectrum of the former does not exhibit the expected $\nu_5(B_2)[\nu_{\text{as}}(\text{NO}_2)]$ and $\nu_1(A_1)[\nu_{\text{s}}(\text{NO}_2)]$ bands for the monodentate nitro groups that are present in the structure, but, instead, it does show the characteristic band of the ionic nitrates at 1380 cm⁻¹ observed in the latter. The appearance of the 1380 cm⁻¹ band in the spectrum of **1a** suggests³ that the monodentate nitro ligands are replaced by bromides that are present in excess in the spectroscopic KBr matrix (this replacement is facilitated by the pressure used for the preparation of the pellet), thus generating ionic nitrates (KNO₃).

1. K. Nakamoto, *Infrared and Raman Spectra of Inorganic and Coordination Compounds*, Wiley, New York, 4th ed., 1986, pp. 121-125, 130-137, 147-155, 248-251, 254-257.
2. C. Papatriantafyllopoulou, E. Manessi-Zoupa, A. Escuer and S. P. Perlepes, *Inorg. Chim. Acta*, 2009, **362**, 634.
3. (a) G. J. Kleywegt, W. G. R. Wiesmeijer, G. J. van Driel, W. L. Driessen, J. Reedijk and J. H. Noordik, *J. Chem. Soc., Dalton Trans.*, 1985, 2177; (b) E. Katsoulakou, V. Bekiari, C. P. Raptopoulou, A. Terzis, P. Lianos, E. Manessi-Zoupa and S. P. Perlepes, *Spectrochim. Acta, Part A*, 2005, **61**, 1627; (c) A. A. Kitos, C. G. Efthymiou, M. J. Manos, A. J. Tasiopoulos, V. Nastopoulos, A. Escuer and S. P. Perlepes, *Dalton Trans.*, 2016, **45**, 1063.

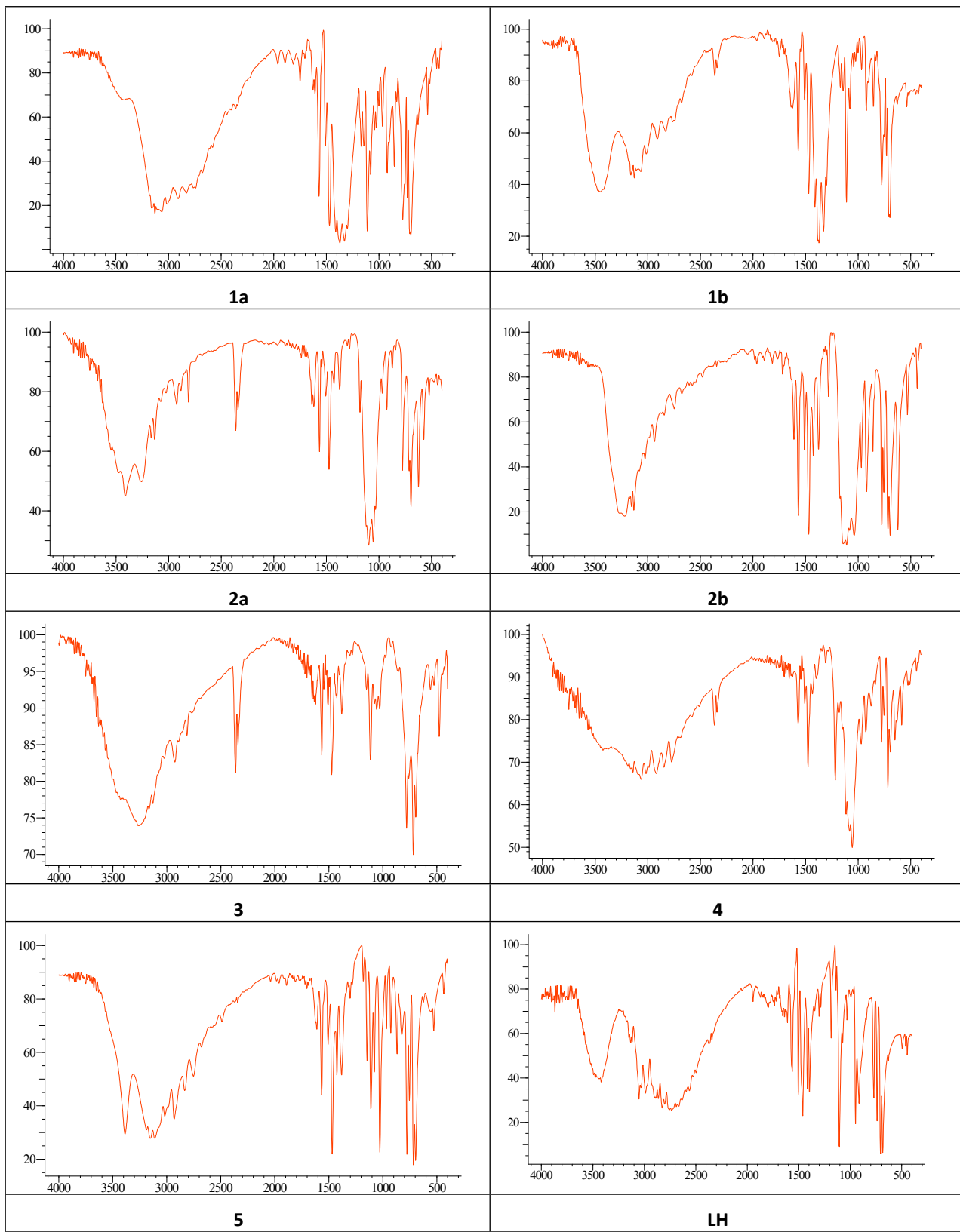


Figure S2. IR spectra for compounds **1a–5** and the free ligand **LH**.